Geophys. J. R. astr. Soc. (1981) 64, 705–727

The forced nutations of an elliptical, rotating, elastic and oceanless earth

John M. Wahr* *Cooperative Institute for Research in Environmental Sciences, University of Colorado, National Oceanic and Atmospheric Administration, Boulder, Colorado 80309, USA*

Received 1980 July 18; in original form 1980 March 10

Summary. We compute the luni-solar forced nutations of an elliptical, rotating, self-gravitating, elastic, hydrostatically prestressed and oceanless earth. Several recent structural models are considered, each possessing a fluid outer core and solid inner core. Complete results are given for the nutation of the 'axis of figure for the Tisserand mean surface' which best represents the observational effects of the Earth's nutational motion. Differences between results for different structural models are observationally insignificant. Differences between our results and Molodensky's are as large as ~ 0.002 arcsec at six month and at 18.6 yr.

1 Introduction

If the Earth were not subject to internal or external stimuli it would rotate rigidly about a fixed axis in space with invariant angular velocity. Of course, the Earth does not exhibit this simple equilibrium behaviour. Of the many processes which affect its rotation, probably the best understood is the combined gravitational force of the Sun and Moon. As seen from the Earth, this force is the sum of a constant term, contributing only to the Earth's orbital behaviour, and a relatively small remainder defined as the luni-solar tidal force. The tidal force, which also causes the ocean and bodily tides, exerts a net torque on the elliptical Earth about an axis perpendicular to the equilibrium rotation axis. The Earth responds to this torque by 'precessing' in space just as a top precesses about the direction of local gravity.

The Earth's motion is considerably complicated by the fact that the axis of precession is not fixed in space but depends on the instantaneous positions of the Sun and Moon relative to the Earth. The resulting motion is quite complicated but can conveniently be described as the sum of two motions. One is the large uniform 'precession of the equinoxes' (see, e.g. Munk & MacDonald 1960) about the normal to the ecliptic plane – a fixed axis in space

*Present address: Geophysical Fluid Dynamics Program, Department of Geological and Geophysical Sciences, Princeton University, Princeton, New Jersey 08544, USA.

determined by the mean positions of the Sun and Moon. The period of this precession is ~ 26 000 yr and the precession angle (between the ecliptic normal and the Earth's rotation axis) is 23.5°. This motion is very important astronomically but since it does not depend on the Earth's detailed mechanical structure or dynamical behaviour, its observation cannot offer much geophysical information. We do not consider the precession of the equinoxes in this paper.

Secondly, superimposed on the precession of the equinoxes are smaller, relatively high-frequency (with periods of from ~ 10 day to 18.6 yr as seen in inertial space) variations in the Earth's angular orientation known as the luni-solar forced nutations. These motions can be interpreted as corrections to the precession due to the motions of the Sun and Moon. Astronomical observations of the nutations are potentially valuable geophysically since the nutations depend on details of the Earth's internal constitution and are caused by a very well-understood external force.

The earliest nutation theories modelled the Earth as a rigid ellipsoid (see, e.g. Woolard 1953). In this approximation only the Earth's principal moments of inertia and the amplitude and frequency of the tidal force are important. Amplitudes are largest at frequencies of 18.6 yr and six month where the angular motion of the pole is ~ 10 and ~ 0.5 arcsec respectively. Currently the most accurate rigid body theory is Kinoshita's (1977).

Jeffreys & Vicente (1957a, b) and Molodensky (1961) greatly extended these results by including the effects of a fluid core and of elasticity within the mantle. They found differences from the rigid earth results of as much as 0.02 arcsec at 18.6 yr and at six months, due primarily to resonant effects in the fluid core. Although these corrections for non-rigidity are smaller than the rigid results, they are well within current observational accuracy (see, e.g. Melchior 1971; Sasao, Okamoto & Sakai 1977; Kinoshita *et al.* 1979; also Section 3 below). In both of these theories mantle deformation is computed for a spherical non-rotating shell and only particularly simple core structures are considered. Furthermore, both calculations rely almost totally on analytical techniques which introduce additional approximations.

Shen & Mansinha (1976) and Sasao, Okubo & Saito (1980) further extended these results to include more complete dynamical and structural models of the fluid core. Sasao *et al.* (1980) use a predominantly analytical approach conceptually similar, in many respects, to that of Molodensky (1961). Shen & Mansinha (1976), relying more heavily on numerical techniques, were able to include even more general representations of the flow in the fluid core. In both cases mantle deformation was computed for a spherically stratified, non-rotating solid shell.

The work described below is a further extension of these results which accounts more completely for the Earth's ellipticity and rotation. The techniques we use were developed by Smith (1974) and Wahr (1981a). Smith (1974) described the linearized equation of infinitesimal motion for a rotating, slightly elliptical, self-gravitating, elastic, hydrostatically prestressed and oceanless earth. Smith (1976, 1977) applied these equations to investigate portions of the Earth's low-frequency normal mode spectrum. Wahr (1981a) demonstrated that the forced motion of a rotating earth could be expanded as a decoupled sum of normal modes of the Earth. Wahr (1981b) used this normal mode expansion together with the linearized equations of Smith (1974) to compute the complete response of the Earth to the luni-solar tidal force. Results of that computation for the induced deformation (i.e. the body tide) and changes in the length of day were discussed by Wahr (1981b) and Wahr, Sasao & Smith (1981), respectively. Results for the Earth's nutational motion are given below. Here, unlike in earlier theories, elliptical and rotational effects are considered throughout the

Earth. Calculations are performed for some of the most heavily constrained elastic earth models currently available, all of which have a fluid outer core and a solid inner core.

In Section 2 we review the computational theory and discuss the nutation of a rigid earth. In Section 3 we discuss the effects of non-rigidity and describe the results. A discussion of these results is presented in Section 4.

2 Rigid earth results

2.1 GENERAL CONSIDERATIONS

The Earth's forced nutations are adequately described as infinitesimal deviations from an equilibrium state of uniform rotation induced by the luni-solar tidal force. To represent the equilibrium state we adopt here a coordinate system, $\mathscr{F}$, centred on the Earth's centre of mass with its $\hat{\mathbf{z}}$-axis oriented along the Earth's mean rotation axis, and rotating about the $\hat{\mathbf{z}}$-axis with angular velocity $\Omega = 7.292115 \times 10^{-5}\,\mathrm{rad\,s^{-1}}$. This coordinate system is thus defined to be independent of any future rotational or deformational motion of the Earth. All discussion below will refer to this system unless otherwise noted.

The luni-solar gravitational force on the Earth consists of a dominant portion which determines the Earth's orbit in space, plus a small remainder which does not affect the Earth's centre of mass. The remainder is the luni-solar tidal force, which at any point $\mathbf{x}$ in the rotating Earth is given by

$$\mathbf{f}(\mathbf{x}, t) = \rho(\mathbf{x})\, \nabla V(\mathbf{x}, t) \tag{2.1}$$

where $\rho(\mathbf{x})$ is the equilibrium mass density at $\mathbf{x}$ and V is the tidal potential (i.e. the negative of the tidal potential energy) with the form

$$V(\mathbf{x}, t) = \sum_{l=2}^{\infty} \sum_{m=0}^{l} c_l^m(t)\, Y_l^m(\theta, \phi) \left(\frac{r}{a}\right)^l g \tag{2.2}$$

where θ and ϕ are colatitude and east longitude, the Y_l^m are spherical harmonics with normalization chosen to coincide with that of Cartwright & Tayler (1971), $a = 6371$ km is the Earth's mean spherical radius, and $g = 982.03\ \mathrm{cm\,s^{-2}}$ is the gravitational acceleration at the mean spherical surface (see, e.g. Bartels 1957, Cartwright & Tayler 1971 and Melchior 1978 for detailed discussions of the tidal force). The $c_l^m(t)$ in (2.2) are conveniently represented in the frequency domain as

$$c_l^m(t) = \sum_{\omega} H_l^m(\omega) \exp\left[\!\left[\mathrm{i}\left[\omega t + \alpha(\omega)\right]\right]\!\right] \tag{2.3}$$

where the sum over ω is over a band of frequencies closely grouped around $m\Omega$, and $\alpha(\omega)$ is the phase at the epoch $t = 0$ (throughout this paper a positive frequency will correspond to retrograde motion: i.e. in the opposite direction of $\boldsymbol{\Omega}$). The H_l^m in (2.3) decrease rapidly with l. For most problems only the $l = 2$, and occasionally the $l = 3$, terms in (2.2) are ever important. Furthermore, as we shall see, only the $l = 2$, $m = 1$ terms in (2.2) can cause nutational motion of an ellipsoidally symmetric earth.

To compute the Earth's response to the tidal force (2.1) we assume that the density distribution $\rho(\mathbf{x})$ is perfectly axially symmetric about the $\hat{\mathbf{z}}$-axis. In this case no external gravitational force can torque the Earth about the $\hat{\mathbf{z}}$-axis. Wahr (1981a) showed that in the frequency domain the response $\mathbf{s}(\mathbf{x}, \omega)$ of the rotating Earth to any force $\mathbf{f}(\mathbf{x}, \omega)$ which neither torques the Earth about the $\hat{\mathbf{z}}$-axis nor displaces the Earth's centre of mass has the

form

$$\mathbf{s}(\mathbf{x}, \omega) = \sum_n a_n(\omega)\mathbf{s}_n(\mathbf{x}) \tag{2.4}$$

where the $\mathbf{s}_n(\mathbf{x})$ are normal modes of the rotating Earth, and the coefficients $a_n(\omega)$ are given by

$$a_n(\omega) = \frac{1}{2} \frac{(\mathbf{f}, \mathbf{s}_n)}{(\omega_n - \omega)[\omega_n(\mathbf{s}_n, \mathbf{s}_n) - (\mathbf{s}_n, \mathrm{i}\boldsymbol{\Omega} \times \mathbf{s}_n)]}. \tag{2.5}$$

Here, ω_n is the eigenfrequency of $\mathbf{s}_n$, $\boldsymbol{\Omega} = \Omega\hat{\mathbf{z}}$ is the angular velocity of the coordinate system $\mathscr{R}$, and we have defined

$$(\mathbf{u}, \mathbf{v}) = \int_{V_E} \rho \mathbf{u} \cdot \mathbf{v}^* \tag{2.6}$$

for any two vectors $\mathbf{u}$ and $\mathbf{v}$, where * denotes complex conjugation and V_E is the volume of the Earth. (A term $b_\Delta \hat{\mathbf{z}} \times \mathbf{x}$ from Wahr (1981a) is not included in (2.4) since it does not contribute to nutational motion.)

2.2 NUTATION OF A RIGID EARTH

The normal mode expansion (2.4) can be applied in principle to any non-dissipative model of the Earth's material structure. The example of a rigid earth was considered by Wahr (1981a) and is of interest here since it provides considerable insight into the nutational behaviour of a non-rigid earth.

For a rigid earth there are only two non-trivial normal modes:

(1) The Eulerian free nutation of the rigid Earth (see, e.g. Munk & MacDonald 1960) with a frequency of $\omega_1 = -[(C-A)/A]\,\Omega$ where C and A are the Earth's principal moments of inertia. This mode represents a wobble of the figure axis about the rotation axis and is exactly equivalent to the free nutational motion of a top.

(2) The tilt-over-mode (TOM) with frequency $\omega_2 = \Omega$ (see Dahlen & Smith 1975; Smith 1977). This mode represents sidereal rotation of the Earth about an axis slightly inclined to the $\hat{\mathbf{z}}$-axis of the coordinate system.

The Eulerian free nutation and the TOM have identical eigenfunctions of the form $\mathbf{s}_n(\mathbf{x}) = (\hat{\mathbf{x}} + \mathrm{i}\hat{\mathbf{y}}) \times \mathbf{x}$.

Wahr (1981a) used (2.4) and (2.5) for these two modes to show that the response of the Earth to an external torque

$$\mathbf{N} = (N_x \hat{\mathbf{x}} + N_y \hat{\mathbf{y}}) \exp\,[\mathrm{i}(\omega t + \alpha)] \tag{2.7}$$

is

$$\mathbf{s}(\mathbf{x}, t) = \frac{N_x - \mathrm{i}N_y}{2C\Omega}\left[\frac{1}{\Omega - \omega} + \frac{1}{[(C-A)/A]\Omega + \omega}\right](\hat{\mathbf{x}} + \mathrm{i}\hat{\mathbf{y}}) \times \mathbf{x} \exp\,[\mathrm{i}(\omega t + \alpha)]. \tag{2.8}$$

$\mathbf{s}(\mathbf{x}, t)$ given by (2.8) represents a forced, rigid rotation about an axis perpendicular to $\boldsymbol{\Omega}$. It is not difficult to show that the torque from the tidal force (2.1) is

$$N_x - \mathrm{i}N_y = -\mathrm{i}\frac{C-A}{a^2}\sqrt{\frac{15}{2\pi}}\, gH_2^1(\omega) \exp\,[\mathrm{i}(\omega t + \alpha)]. \tag{2.9}$$

Consequently, only the $l = 2$, $m = 1$ tides can perturb a rigid earth. Since these tides have approximately diurnal frequencies, the TOM contribution to (2.8) (proportional to $1/(\Omega - \omega)$) is nearly resonant and accounts for almost the entire displacement.

To examine the response (2.8) in more detail we consider the accompanying perturbations in the Earth's rotation axis, figure axis and angular momentum axis. Define

$$\mathbf{r}(\mathbf{x}, t) = \mathbf{x} + \mathbf{s}(\mathbf{x}, t) \tag{2.10}$$

as the instantaneous position in $\mathscr{R}$ of the material particle with equilibrium position $\mathbf{x}$. Here, $\mathbf{s}$ is given by (2.8) and has the form

$$\mathbf{s}(\mathbf{x}, t) = \boldsymbol{\xi}_r(\omega) \times \mathbf{x} \exp\,[\mathrm{i}(\omega t + \alpha)] \tag{2.11}$$

where $\boldsymbol{\xi}_r(\omega)$ is the complex rigid rotation

$$\boldsymbol{\xi}_r(\omega) = \frac{N_x - \mathrm{i}N_y}{2C\Omega}\left[\frac{1}{\Omega - \omega} + \frac{1}{[(C-A)/A]\Omega + \omega}\right](\hat{\mathbf{x}} + \mathrm{i}\hat{\mathbf{y}}). \tag{2.12}$$

The rotation axis, $\mathbf{I}$, satisfies

$$\frac{d\mathbf{r}}{dt} = \mathbf{I} \times \mathbf{r}$$

where in our rotating reference frame

$$\frac{d}{dt} = \partial_t + \boldsymbol{\Omega} \times . \tag{2.13}$$

Applying (2.13) to (2.10) gives easily

$$\mathbf{I} = \boldsymbol{\Omega} + \partial_t \boldsymbol{\xi}_r = \Omega\left[\hat{\mathbf{z}} + \mathrm{i}\frac{\omega}{\Omega}\boldsymbol{\xi}_r \exp\,[\mathrm{i}(\omega t + \alpha)]\right]. \tag{2.14}$$

Equation (2.14) describes a periodic change in the orientation of the rotation axis in space ($\boldsymbol{\xi}_r$ is perpendicular to $\hat{\mathbf{z}}$). For each perturbing frequency $\mathbf{I}$ traces out a circular cone about the $\hat{\mathbf{z}}$-axis. This motion in space is called a 'nutation' of the rotation axis. In a similar manner we will describe nutational motion of the figure and angular momentum axes (we will show below that the nutation of a rigid earth is most conveniently associated with the nutation of the figure axis).

The figure axis, $\mathbf{F}$, can be found by noting that for a rigid body $\mathbf{F}$ will always point towards the geographic north pole. The displaced position of the pole is (using (2.10), (2.11) and (2.8))

$$\mathbf{F} = \mathbf{r}(\hat{z}, t) = \hat{\mathbf{z}} + \mathrm{i}\boldsymbol{\xi}_r \exp\,[\mathrm{i}(\omega t + \alpha)]. \tag{2.15}$$

The angular momentum, $\mathbf{H}$, is given by

$$\mathbf{H} = \int_{V_E} \rho(\mathbf{x})\mathbf{r}(\mathbf{x}, t) \times \frac{d}{dt}\mathbf{r}(\mathbf{x}, t) d^3\mathbf{x} \tag{2.16}$$

where $\mathbf{r}(\mathbf{x}, t)$ and d/dt are given by (2.10) and (2.13) respectively. After some algebra (2.16) gives

$$\mathbf{H} = C\Omega\left[\hat{\mathbf{z}} + \frac{A}{C\Omega}\left[\frac{C-A}{A}\Omega + \omega\right]\mathrm{i}\boldsymbol{\xi}_r \exp\,[\mathrm{i}(\omega t + \alpha)]\right]. \tag{2.17}$$

Polar motion, **P**, is defined as the vector displacement between the figure axis, **F**, and the rotation axis, **I**. By comparing (2.14) and (2.15) we find

$$\mathbf{P} = \mathbf{I}/\Omega - \mathbf{F} = \left(\frac{\omega}{\Omega} - 1\right) i\xi_r \exp\,[i(\omega t + \alpha)]. \tag{2.18}$$

At diurnal frequencies ($\omega \approx \Omega$) (2.14), (2.15) and (2.17) show that the rotation, figure and angular momentum axis are very nearly coincident. Furthermore, since ξ_r is resonant at $\omega = \Omega$ due to the TOM contributions (see 2.8), the tidally induced nutations of these axes can be very large. Polar motion (2.18), on the other hand, is *not* resonant at $\omega = \Omega$ and its diurnal tidal excitation is much smaller than the corresponding motion of **I**, **F** or **H**.

2.3 THE EFFECTS OF NUTATION ON ECLIPTIC LONGITUDE AND OBLIQUITY

Equations (2.14), (2.15) and (2.17) describe the instantaneous positions of the axes **I**, **F** and **H** in the rotating coordinate system $\mathscr{R}$. The motion of each of these axes is approximately diurnal, since it is driven by the diurnal component of the tidal force. However, the nutational motion of an axis is more conventionally described as a long-period variation in the ecliptic longitude and obliquity of that axis. To understand the correspondence between ecliptic longitude and obliquity and the results (2.14), (2.15) and (2.17), we consider three related coordinate systems.

First, the geocentric ecliptic system of date, E, is a non-rotating inertial system with origin at the Earth's instantaneous centre of mass. The $\hat{\mathbf{x}}$–$\hat{\mathbf{y}}$ ecliptic plane is defined as the mean plane of the Earth's orbit about the Sun and Moon at some prescribed epoch, t_0, with the $\hat{\mathbf{x}}$-axis oriented along the intersection with the Earth's equatorial plane at epoch (this intersecting line is called the equinox).

Secondly, the Earth's rotating equatorial system, $\mathscr{R}$, is the invariably rotating coordinate system defined in Section 2.1. In this system the $\hat{\mathbf{z}}$-axis is oriented along $\boldsymbol{\Omega}$ (the time-averaged rotation vector at epoch) and the $\hat{\mathbf{x}}$-axis along the equilibrium Greenwich meridian.

Thirdly, the Earth's non-rotating equatorial system, X, is similar to $\mathscr{R}$ except that X is not sidereally rotating. The $\hat{\mathbf{z}}$-axis in X is oriented along the rotation vector, $\boldsymbol{\Omega}$, and the $\hat{\mathbf{x}}$-axis along the equinox.

Each of the axes **I**, **F** and **H** defined in Section 2.2 has a direction in $\mathscr{R}$ of the form

$$\mathbf{A}_{\mathscr{R}} = \hat{\mathbf{z}} + i\delta a(\hat{\mathbf{x}} + i\hat{\mathbf{y}}) \exp\,[i(\omega t + \alpha)] \tag{2.19}$$

where δa is an incremental (real) scalar constant reflecting the tidally induced displacement of $\mathbf{A}_{\mathscr{R}}$. To transform **A** to non-rotating inertial space, X, we rotate (2.19) with the appropriate coordinate transformation

$$\begin{pmatrix} \cos\beta & -\sin\beta & 0 \\ \sin\beta & \cos\beta & 0 \\ 0 & 0 & 1 \end{pmatrix} \tag{2.20}$$

where β is Greenwich mean sidereal time (the angle in the equatorial plane between the equilibrium Greenwich meridian and the equinox)

$$\beta = \Omega t + \alpha_0 \tag{2.21}$$

with α_0 the phase at epoch. Then

$$\mathbf{A}_X = \hat{\mathbf{z}} + i\delta a(\hat{\mathbf{x}} + i\hat{\mathbf{y}}) \exp\,[\![i[(\omega - \Omega)t + \alpha - \alpha_0]]\!]. \tag{2.22}$$

As (2.22) shows, a nearly diurnal tidal frequency, ω, in $\mathscr{R}$ corresponds to a long period, $1/(\omega - \Omega)$, in inertial space, X.

By a tedious but conceptually simple application of successive rotations from X to E, the orientation of **A** relative to the ecliptic plane can be described by two angles: $\epsilon = \epsilon_0 + \delta\epsilon$ and $\psi = \delta\psi$ where

$$\begin{aligned} \delta\epsilon &= -\delta a \exp[\![\mathrm{i}[(\omega - \Omega)t + \alpha - \alpha_0]]\!] \\ \sin\epsilon_0 \delta\psi &= \mathrm{i}\delta a \exp[\![\mathrm{i}[(\omega - \Omega)t + \alpha - \alpha_0]]\!]. \end{aligned} \tag{2.23}$$

The obliquity, ϵ, describes the absolute angle between **A** and the normal to the ecliptic, while the longitude, ψ, is defined as 90° minus the angle in the ecliptic plane between the projection of **A** and the equinox (see Fig. 1). For an unperturbed axis, where $\mathbf{A}_R = \hat{\mathbf{z}}$, we find $\epsilon = \epsilon_0$ and $\psi = 0$.

For every diurnal tidal term with frequency $\omega_+ = \Omega + f$ and phase $\alpha_+ = \alpha_0 + \delta\alpha$ there is a complementary term with frequency $\omega_- = \Omega - f$ and phase $\alpha_- = \alpha_0 - \delta\alpha$. (This symmetrical 'splitting' is due to modulation of the Earth's purely sidereal mean frequency of rotation by the ecliptic motion of the Sun and Moon.) Both these tidal terms have the same apparent frequency in E. Defining δa_+ and δa_- as the amplitudes of δa at these two complementary frequencies and adding together the corresponding perturbations of ϵ and ψ gives

$$\begin{aligned} \delta\epsilon &= -(\delta a_+ + \delta a_-)\cos(ft + \delta\alpha) \\ \sin\epsilon_0 \delta\psi &= -(\delta a_+ - \delta a_-)\sin(ft + \delta\alpha). \end{aligned} \tag{2.24}$$

Equation (2.24) implies that a_+ and a_-, which are two diurnal circular nutations in $\mathscr{R}$, combine to produce a long-period elliptical nutation in non-rotating inertial space.

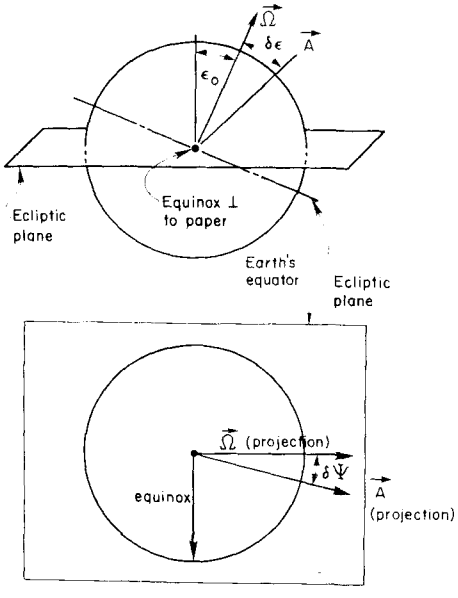

Figure 1. The top half shows the ecliptic obliquity ($\epsilon_0 + \delta\epsilon$) of the vector **A**. ϵ_0 is the obliquity of the mean rotation vector $\boldsymbol{\Omega}$, and $\delta\epsilon$ is assumed to be small. Also shown are the relative orientations of the Earth's non-rotating equatorial coordinate system and the ecliptic coordinate system. The lower half shows the ecliptic longitude ($\delta\Psi$) of the vector **A**. $\delta\Psi$ is assumed to be small.

There are sound practical reasons to describe the nutations with $\delta\epsilon$ and $\delta\psi$ rather than with δa_+ and δa_-. Classical astronomical observations are sensitive to the orientation of the stars relative to the nutating Earth, and tabulated star positions are readily available in the ecliptic system. Nutational variations of $\delta\epsilon$ and $\delta\psi$ can thus be used to rotate the star positions from the ecliptic to an earth-fixed system (or vice versa).

There has been some confusion, however, as to which polar axis (**I**, **F** or **H**) should be used to represent the rigid earth. Jeffreys (1959) and Atkinson (1973, 1975) correctly pointed out that since for observational purposes the axis should be attached to the observatories, the most desirable axis to use is the figure axis. As shown in (2.15), nutations of the figure axis directly reflect perturbations in ξ_r which, in turn, determine the displacement of any point on the rigid earth (see 2.1). It is these displacements which ultimately affect observations. If, instead, the rotation axis were used, corrections would have to be made for the factor ω/Ω in (2.14). This is equivalent to correcting for diurnal polar motion (see 2.18) or for the 'dynamical variation of latitude' (see, e.g. Atkinson 1973). Similar corrections would be necessary if the angular momentum axis were used.

3 Nutation of a non-rigid earth

3.1 GENERAL DISCUSSION

The response of the real Earth to the $l = 2, m = 1$ tidal force is considerably complicated by non-rigidity. The induced displacement field contains not only nutational motion but also deformation, i.e. the body tide. Furthermore, the nutation angle is not necessarily constant throughout the Earth. We will show, in fact, that there is a large discontinuity in nutation angle across the core–mantle boundary.

Wahr (1981b) used the normal mode expansion described briefly in Section 2.1 to compute the tidal response of a rotating, elliptical, self-gravitating, elastic and oceanless earth. He showed that for an $l = 2$, $m = 1$ tide with (diurnal) frequency ω, the induced displacement at any point, $\mathbf{x}$, has the form (in $\mathscr{H}$)

$$s(\mathbf{x}, \omega) = \eta(r, \omega)\,(\hat{\mathbf{x}} + i\hat{\mathbf{y}}) \times \mathbf{x} + \mathbf{b}(\mathbf{x}, \omega) \tag{3.1}$$

where $\eta(r, \omega)$ is the radially dependent nutation angle and $\mathbf{b}(\mathbf{x}, \omega)$ is the body tide displacement. The separation between the nutational and body tide components in (3.1) is uniquely defined by the requirement that $\eta(r, \omega)$ represent the best least-squares fit of a nutational displacement to $\mathbf{s}(\mathbf{x}, \omega)$ over the spherical shell $|\mathbf{x}| = r$. We discuss here results for $\eta(r, \omega)$ and their observational significance. Results for the body tide, $\mathbf{b}(\mathbf{x}, \omega)$ are discussed by Wahr (1981b).

One of the common objectives of this study and of Wahr (1981b) is to determine whether observations either of the forced nutations or the body tide can extend our knowledge of the Earth's deep interior. For this reason we have computed results for η and $\mathbf{b}$ for several structural models of the Earth. Although recent advances in seismology have greatly improved our knowledge of the Earth's material structure, the important stability of the fluid core is still largely unknown. The stability is characterized by the squared Brunt-Väisälä frequency, N^2 (see, e.g. Masters 1979). Masters (1979) concluded that the core is nearly neutrally stable ($N^2 = 0$) except possibly near the core–mantle boundary where it may be positively stable ($N^2 > 0$). Nutation results will be discussed here for four structural models: (1) model 1066A of Gilbert & Dziewonski (1975), (2) model PEM-C of Dziewonski, Hales & Lapwood (1975); and two variants of 1066A obtained by modifying slightly the density structure in the fluid core so that the core is (3) neutrally stratified, (4) positively stable ($N^2 = 8.1 \times 10^{-9}\,\mathrm{s}^{-2}$). (See Wahr (1981b) for further discussion of these models.)

To apply successfully the eigenfunction expansion (2.4) we require detailed knowledge of the normal modes of an elliptical, rotating, non-rigid earth. Briefly, the set of modes most pertinent to this study and discussed below are the free oscillations, the tilt-over-mode (TOM), the free core nutation (FCN) (often referred to as the nearly diurnal free wobble) and the Chandler wobble (CW) (see Wahr (1981a, b) for a more complete summary of the normal mode set). The displacement field for each of these modes has the general form

$$\mathbf{s}_n(\mathbf{x}) = \eta_n(r)\,(\hat{\mathbf{x}} + i\hat{\mathbf{y}}) \times \mathbf{x} + \mathbf{b}_n(\mathbf{x}) \tag{3.2}$$

where η_n and $\mathbf{b}_n$ represent the nutational and deformational displacements, respectively, of mode. Using (3.2) in the expansion (2.4) gives an expansion for the forced nutations:

$$\eta(r, \omega) = \sum_n a_n(\omega)\eta_n(r). \tag{3.3}$$

Consequently, the effect of any mode on the nutations depends critically on η_n for that mode.

The elastic free oscillations (all of which have periods $\leqslant$ 1 hr) are mostly descriptive of deformation $(r\eta_n(r)/|\mathbf{b}_n(\mathbf{x})| \ll 1)$, and consequently their contribution to (3.3) is small. On the other hand, the TOM, FCN and CW have large η_n components. The TOM for a non-rigid earth is identical to the TOM for a rigid earth as described above in Section 2.2: η_n is independent of r, $\mathbf{b}_n = 0$ and the eigenfrequency = Ω. The CW corresponds to the Eulerian free nutation of a rigid earth as discussed in Section 2.2. However, in the non-rigid case $\eta_n(r)$ nearly vanishes in the fluid core ($\eta_n(r)$ is still nearly constant throughout the mantle), $\mathbf{b}_n$ is no longer 0 (although $|\mathbf{b}_n(\mathbf{x})|/[r\eta_n(r)] \approx 1/300$) and the period is increased from ~ 305 day (rigid case) to ~ 396 day (see, e.g. Smith & Dahlen 1981). The FCN is a free retrograde motion due primarily to the fluid outer core of the Earth. It consists of a nearly radially independent nutation in the mantle and a larger nutation in the opposite direction in the fluid core. The deformation, $\mathbf{b}_n$, is non-zero (although $|\mathbf{b}_n(\mathbf{x})|/[r\eta_n(r)] \approx 1/300$) and the eigenfrequency is $\approx (1 + 1/460)$ cycle sidereal day^{-1}.

Since η_n for both the CW and the FCN is discontinuous across the core–mantle boundary, we anticipate from (3.3) that the forced nutation angle, η, is also discontinuous. In this case there will be no single value of η which can simultaneously characterize all nutational displacements within the Earth. Since all observations are made at the outer surface, we will uniquely identify the Earth's nutation with the nutation angle evaluated at the mean spherical surface: $\eta(a, \omega)$. The total diurnal tidal displacement of any observatory is then the sum of the body tide displacement, $\mathbf{b}(a, \omega)$, and the nutational displacement as characterized by $\eta(a, \omega)$. The significance of this 'definition' of nutation is that once a set of astrometric data is corrected for the effects of the body tide, the remainder can be identified uniquely as nutation and compared with the results for $\eta(a, \omega)$ described below. If any other angle were chosen to describe the nutations, additional corrections to the data would be necessary, in principle at least, to adjust back to the surface values.

3.2 COMPUTATION

The simultaneous computation of $\eta(a, \omega)$ and $\mathbf{b}(a, \omega)$ induced by the $l = 2$, $m = 1$ tides is described by Wahr (1981b). To minimize the computational effort he used a variation of the expansion (2.4) where the equations of motion were first integrated directly at the frequency of the O_1 tide, $\omega_{O_1} = (0.927)\Omega$, and then (2.4) was used to find differences at other frequencies.

In this case, assuming an external tidal potential of the form (2.1)–(2.3), $\eta(a, \omega)$ is given in radians by

$$\eta(a, \omega) = \left[A_0 + (\omega - 0.927\Omega)\left[-\frac{10.044}{\Omega - \omega} + \frac{A_1}{\omega_1 - \omega} + \frac{A_2}{\omega_2 - \omega}\right]\right] i\left(\frac{H_2^1(\omega)}{a}\right). \tag{3.4}$$

Here, ω_1 and ω_2 are the eigenfrequencies of the CW and FCN respectively, and A_0, A_1 and A_2 are frequency-independent constants which depend on the material structure within the Earth. (The TOM coefficient, -10.044, was computed using $(C-A)/C = 0.003273952$ from Kinoshita (1977).) We have computed A_0, A_1, A_2, ω_1 and ω_2 for the four earth models described above. Results for these models are shown in Table 1. Although differences between the models may be near the level of computational accuracy, they are certainly far too small to detect observationally, as we discuss below.

Table 1. Shows the eigenfrequencies of the CW (ω_1/Ω cycle sidereal day^{-1}) and the FCN (ω_2/Ω cycle sidereal day^{-1}) and values of the expansion coefficients used in (3.4) and (3.6). Results are shown for four structural models of the Earth.

Model	ω_1/Ω ($\times 10^{-3}$)	ω_2/Ω	A_0	A_1	A_2	B_0	B_1	B_2
1066A	−2.478	1.0021714	−11.12	−0.596	−0.489	0.416	0.810	0.665
Neutral 1066A	−2.478	1.0021716	−11.12	−0.596	−0.491	0.418	0.810	0.667
Stable 1066A	−2.479	1.0021708	−11.12	−0.596	−0.490	0.418	0.810	0.667
PEM-C	−2.480	1.0021771	−11.11	−0.599	−0.490	0.417	0.814	0.666

Frequency-dependent results for $\eta(a, \omega)$ are shown in Fig. 2 for model 1066A. These results assume that $H_2^1(\omega)$ is independent of frequency. The TOM has by far the largest effect on $\eta(a, \omega)$ and is shown separately in Fig. 2. Its (resonant) contribution to $\eta(a, \omega)$ is proportional to the total luni-solar torque on the Earth. The remaining effects consist of a

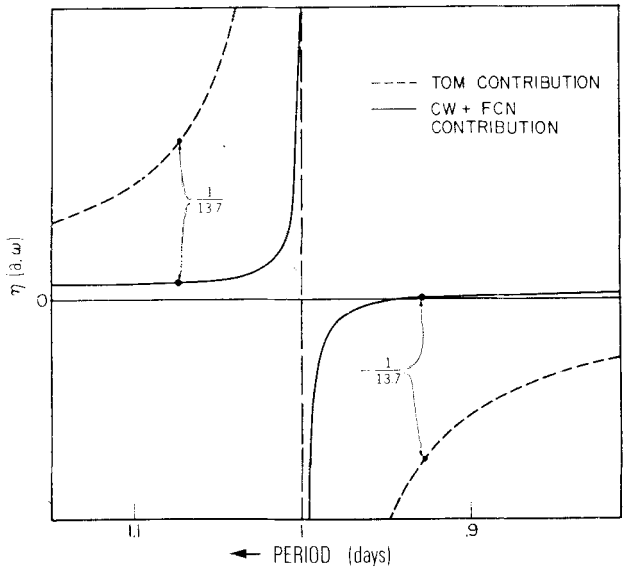

Figure 2. Results for $\eta(a, \omega)$ are shown as a function of period as computed for model 1066A. The perturbing gravitational force is assumed to be independent of period. The large TOM contribution is shown separately.

narrow resonance at the FCN eigenfrequency superimposed on a small positive offset: the CW contribution to (3.4) (frequency-dependent contributions from other modes are too small to be included in (3.4) or in Fig. 2). Since the FCN consists of a differential rotation between the core and mantle, its contribution to (3.4) is sensitive to the *difference* between the external torques on the core and mantle. Since the differential torque due to the tidal force is small compared to the total torque, the FCN resonance in Fig. 2 is much narrower than the TOM resonance. The effect of the CW is small and nearly constant simply because the CW eigenfrequency is far from the diurnal tidal band.

An accurate assessment of the luni-solar forced nutations using (3.4) requires accurate knowledge of the potential coefficients, $H_2^1(\omega)$. However, the most convenient way to include the tidal potential is not to specify directly the $\{H_2^1(\omega)\}$, but to use a rigid earth nutation series which has an accurate potential theory built into it. For this purpose we consider the ratio $\eta(a, \omega)/\eta_r(\omega)$, where

$$\xi_r(\omega) = \eta_r(\omega)(\hat{x} + i\hat{y}) \tag{3.5}$$

is the nutation angle for a rigid earth as described by (2.12). It is evident that $H_2^1(\omega)$ will divide out of η/η_r. Using (2.8), (2.9) and (3.4) we find that

$$\frac{\eta(a,\omega)}{\eta_r(\omega)} - 1 = \left[B_0 + (\omega - 0.927\Omega)\left[\frac{B_1}{\omega_1 - \omega} + \frac{B_2}{\omega_2 - \omega} + \frac{1.06}{\omega + 3.28 \times 10^{-3}\Omega}\right]\right] \times \left[\frac{\Omega - \omega}{\Omega}\right]\left[\frac{\omega}{\Omega} + 3.28 \times 10^{-3}\right] \tag{3.6}$$

where B_0, B_1 and B_2 are frequency-independent constants shown in Table 1 for the four structural models considered here. Again, differences between results for the different models are small.

$(\eta/\eta_r) - 1$ is shown in Fig. 3 as a function of (diurnal) period for model 1066A. The pronounced resonance in $(\eta/\eta_r) - 1$ is due to the FCN contribution to (3.6). The TOM resonance is no longer evident since it has identical effects on η and η_r. The constant background slope and the zero crossing at exactly one sidereal day merely reflect division by η_r.

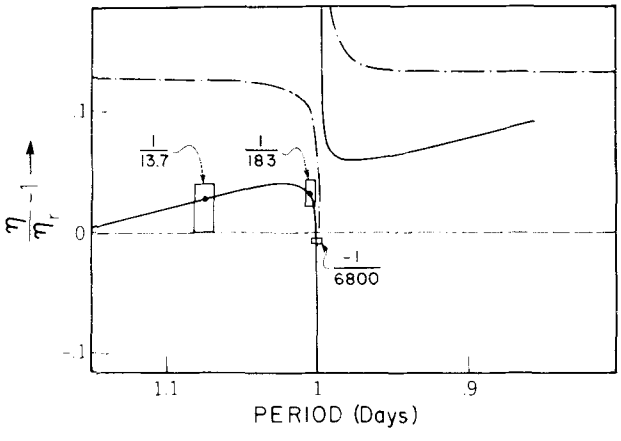

Figure 3. Results for $(\eta/\eta_r) - 1$ are shown as a function of period for model 1066A (——), for the Poincare model: a rigid mantle enclosing a homogeneous, incompressible fluid core (— · —), and for a rigid earth (– – –). The boxed areas include the observational results for 1/13.7, 1/183 and – 1/6800, and are amplified in Fig. 4. The Poincare and rigid earth models are evidently inconsistent with the observations.

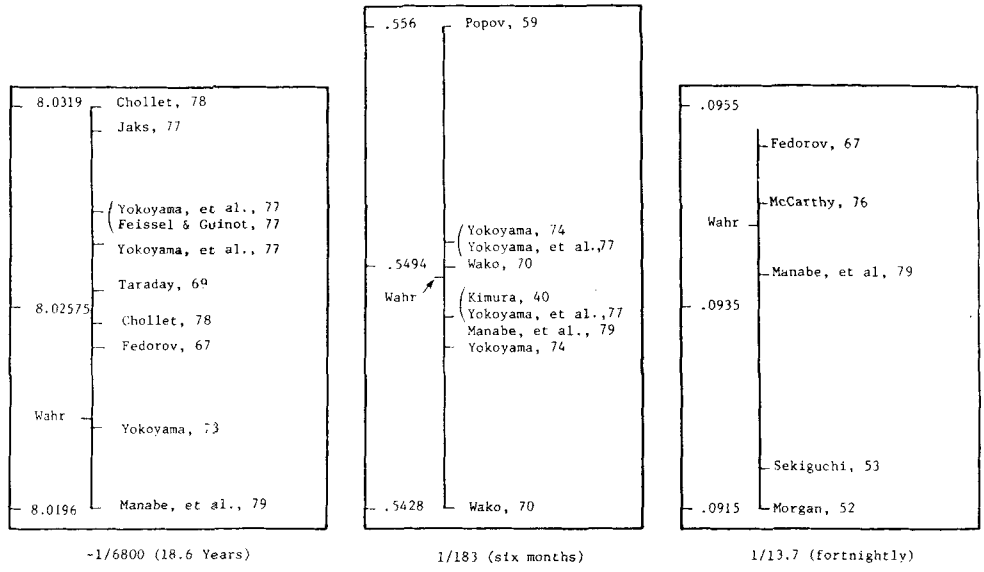

Figure 4. Observed circular nutation amplitudes in arcseconds are compared with the results computed here. The observed results are from Kinoshita *et al.* (1979). The theoretical results (Wahr) are computed by convolving the rigid earth results given by Kinoshita *et al.* (1979) with the non-rigid corrections computed here.

Also shown in Fig. 3 are the results for both a rigid earth ($\eta = \eta_r$) and for an earth with a homogeneous, incompressible fluid core and a rigid mantle (the Poincare (1910) model – see, e.g. Sasao *et al.* 1977). The boxed areas in Fig. 3 are converted to absolute arcsecond amplitudes for $\eta(a, \omega)$ and compared with observational results in Fig. 4. (There are many possible ways to label the circular nutation components, $\eta(a, \omega)$. In Figs 4 and 5 and Tables 3 and 4 we identify the 18.6 yr, annual, semi-annual and fortnightly nutations with $\pm 1/6800$, $\pm 1/365$ and $\pm 1/13.7$, respectively, which roughly correspond to the approximate nutation frequencies in cycle per solar day as seen from non-rotating inertial space. A minus sign corresponds to retrograde nutational motion, i.e. in the opposite direction of Ω). The observed values in Fig. 4 are from Kinoshita *et al.* (1979). Although the observations are consistent with the results computed here and in evident conflict with the rigid earth and Poincare results, the scatter between measurements is too large to differentiate between different theoretical results, as discussed below.

Results computed with (3.6) could be convolved with rigid earth results for η_r to find $\eta(a, \omega)$ as a function of frequency (as was done to generate the theoretical results shown in Fig. 4). However, as discussed in Section 2.3, nutation results are conventionally expressed as variations in longitude and obliquity of some axis characterizing the Earth. To find these variations we note that the nutational displacement component in (3.1) has the form $\xi(a, \omega) \times \mathbf{x}$, where

$$\xi(a, \omega) = \eta(a, \omega)(\hat{\mathbf{x}} + i\hat{\mathbf{y}}). \tag{3.7}$$

This displacement is representative of a purely *rigid* rotation of the mean spherical surface. Consequently, the purely kinematical relationships developed in Section 2.3 between longitude and obliquity variations and the nutation angle, ξ_r, for a rigid earth are also applicable here for $\xi(a, \omega)$. Following the discussion at the end of Section 2.3, we note that

the axis which most directly represents the nutational displacement of the surface, and which consequently is the most appropriate axis to describe the Earth's nutation, is

$$\mathbf{B}(\omega) = \hat{\mathbf{z}} + i\xi(a, \omega) \tag{3.8}$$

corresponding to (2.15) for the figure axis of a rigid earth. It should be understood that **B** is *not* the figure axis for a tidally displaced non-rigid earth, since (1) the rotation angle $\xi(r, \omega)$ depends on r, and (2) the body tide **b** in (3.1) perturbs the figure axis but has no effect on **B**. The physical significance of the axis **B** is described in Section 3.3. (The nutation of the figure axis is also discussed for comparison.)

Ecliptic variations in longitude and obliquity for **B** are expressed in terms of $\eta^+(f) = \eta(a, \Omega + f)$ and $\eta^-(f) = \eta(a, \Omega - f)$ with equations analogous to (2.24):

$$\begin{aligned} \delta\epsilon &= -(\delta\eta^+ + \delta\eta^-)\cos(ft + \alpha) \\ \sin\epsilon_0\delta\psi &= -(\delta\eta^+ - \delta\eta^-)\sin(ft + \alpha). \end{aligned} \tag{3.9}$$

Using (3.9) and (2.24) we can express the variations in longitude ($\delta\psi$) and obliquity ($\delta\epsilon$) of **B** in terms of $\delta\epsilon_r$, $\delta\psi_r$ for the figure axis of a rigid earth. We find

$$\begin{aligned} \delta\epsilon &= \delta\epsilon_r \frac{1}{2}\left[\frac{\eta^+}{\eta_r^+} + \frac{\eta^-}{\eta_r^-}\right] + \sin\epsilon_0\delta\psi_r \frac{1}{2}\left[\frac{\eta^-}{\eta_r^-} - \frac{\eta^+}{\eta_r^+}\right] \\ \sin\epsilon_0\delta\psi &= \delta\epsilon_r \frac{1}{2}\left[\frac{\eta^+}{\eta_r^+} - \frac{\eta^-}{\eta_r^-}\right] + \sin\epsilon_0\delta\psi_r \frac{1}{2}\left[\frac{\eta^+}{\eta_r^+} + \frac{\eta^-}{\eta_r^-}\right]. \end{aligned} \tag{3.10}$$

We have used (3.10) to convolve results for η^+/η_r^+ and η^-/η_r^- computed from (3.6) with results for $\delta\epsilon_r$ and $\delta\psi_r$ from Kinoshita's (1977) rigid earth theory. Specifically, we have used results for the figure axis computed by Kinoshita *et al.* (1979) using orbital elements at the epoch 2000 (these elements correspond to the current IAU system of astronomical constants). The resulting perturbations in $\delta\epsilon$ and $\sin\epsilon_0\delta\psi$ for the axis **B** are shown in Table 2 in units of 0.0001 arcsec. Here, the arguments (l, l', F, D, Ω) are the conventionally adopted arguments after Brown (1919), and the period in solar days is the nutational period as seen from non-rotating inertial space.

3.3 NUTATIONS OF OTHER AXES

The axis **B** was defined above to represent the Earth's nutational motion because it is most directly related to nutational observations. Other axes, however, can be defined and their induced motion computed. The results provide insight into the tidally induced behaviour of the Earth.

Mean rotation vector

The total tidally induced displacement vector at any point **x** in the Earth is $\mathbf{s}(\mathbf{x}, \omega)$ given by (3.1). Since a rigid change in rotation corresponds to a displacement of the form $\bar{\boldsymbol{\xi}} \times \mathbf{x}$, we follow Jeffreys (1970) and define the mean rotation vector of the Earth as

$$\mathbf{I}_E = \boldsymbol{\Omega} + \partial_t \bar{\boldsymbol{\xi}} \tag{3.11}$$

Table 2. Nutation in ecliptic longitude and obliquity of the axis **B** computed for epoch J 2000.0 (JED 2451545.0). T is given in Julian centuries. The results represent a convolution of the rigid earth results given by Kinoshita *et al.* (1979) with the non-rigid corrections computed here. Each nutation term is represented by a particular combination of the fundamental arguments l, l', F, D, Ω. The corresponding period is given in solar days.

	Argument					Period	Longitude		Obliquity	
	l	l'	F	D	Ω	(day)	(0.0001 arcsec)		(0.0001 arcsec)	
1	0	0	0	0	1	6798.4	−171996	−174.2T	92025	8.9T
2	0	0	0	0	2	3399.2	2062	0.2T	−895	0.5T
3	−2	0	2	0	1	1305.5	46	0.0T	−24	0.0T
4	2	0	−2	0	0	1095.2	11	0.0T	0	0.0T
5	−2	0	2	0	2	1615.7	−3	0.0T	1	0.0T
6	1	−1	0	−1	0	3232.9	−3	0.0T	0	0.0T
7	0	−2	2	−2	1	6786.3	−2	0.0T	1	0.0T
8	2	0	−2	0	1	943.2	1	0.0T	0	0.0T
9	0	0	2	−2	2	182.6	−13187	−1.6T	5736	−3.1T
10	0	1	0	0	0	365.3	1426	−3.4T	54	−0.1T
11	0	1	2	−2	2	121.7	−517	1.2T	224	−0.6T
12	0	−1	2	−2	2	365.2	217	−0.5T	−95	0.3T
13	0	0	2	−2	1	177.8	129	0.1T	−70	0.0T
14	2	0	0	−2	0	205.9	48	0.0T	1	0.0T
15	0	0	2	−2	0	173.3	−22	0.0T	0	0.0T
16	0	2	0	0	0	182.6	17	−0.1T	0	0.0T
17	0	1	0	0	1	386.0	−15	0.0T	9	0.0T
18	0	2	2	−2	2	91.3	−16	0.1T	7	0.0T
19	0	−1	0	0	1	346.6	−12	0.0T	6	0.0T
20	−2	0	0	2	1	199.8	−6	0.0T	3	0.0T
21	0	−1	2	−2	1	346.6	−5	0.0T	3	0.0T
22	2	0	0	−2	1	212.3	4	0.0T	−2	0.0T
23	0	1	2	−2	1	119.6	4	0.0T	−2	0.0T
24	1	0	0	−1	0	411.8	−4	0.0T	0	0.0T
25	2	1	0	−2	0	131.7	1	0.0T	0	0.0T
26	0	0	−2	2	1	169.0	1	0.0T	0	0.0T
27	0	1	−2	2	0	329.8	−1	0.0T	0	0.0T
28	0	1	0	0	2	409.2	1	0.0T	0	0.0T
29	−1	0	0	1	1	388.3	1	0.0T	0	0.0T
30	0	1	2	−2	0	177.5	−1	0.0T	0	0.0T
31	0	0	2	0	2	13.7	−2274	−0.2T	977	−0.5T
32	1	0	0	0	0	27.6	712	0.1T	−7	0.0T
33	0	0	2	0	1	13.6	−386	−0.4T	200	0.0T
34	1	0	2	0	2	9.1	−301	0.0T	129	−0.1T
35	1	0	0	−2	0	31.8	−158	0.0T	−1	0.0T
36	−1	0	2	0	2	27.1	123	0.0T	−53	0.0T
37	0	0	0	2	0	14.8	63	0.0T	−2	0.0T
38	1	0	0	0	1	27.7	63	0.1T	−33	0.0T
39	−1	0	0	0	1	27.4	−58	−0.1T	32	0.0T
40	−1	0	2	2	2	9.6	−59	0.0T	26	0.0T
41	1	0	2	0	1	9.1	−51	0.0T	27	0.0T
42	0	0	2	2	2	7.1	−38	0.0T	16	0.0T
43	2	0	0	0	0	13.8	29	0.0T	−1	0.0T
44	1	0	2	−2	2	23.9	29	0.0T	−12	0.0T
45	2	0	2	0	2	6.9	−31	0.0T	13	0.0T
46	0	0	2	0	0	13.6	26	0.0T	−1	0.0T
47	−1	0	2	0	1	27.0	21	0.0T	−10	0.0T
48	−1	0	0	2	1	32.0	16	0.0T	−8	0.0T
49	1	0	0	−2	1	31.7	−13	0.0T	7	0.0T
50	−1	0	2	2	1	9.5	−10	0.0T	5	0.0T
51	1	1	0	−2	0	34.8	−7	0.0T	0	0.0T

Table 2.–*Continued*

	Argument					Period	Longitude		Obliquity	
	l	l'	F	D	Ω	(day)	(0.0001 arcsec)		(0.0001 arcsec)	
52	0	1	2	0	2	13.2	7	0.0T	−3	0.0T
53	0	−1	2	0	2	14.2	−7	0.0T	3	0.0T
54	1	0	2	2	2	5.6	−8	0.0T	3	0.0T
55	1	0	0	2	0	9.6	6	0.0T	0	0.0T
56	2	0	2	−2	2	12.8	6	0.0T	−3	0.0T
57	0	0	0	2	1	14.8	−6	0.0T	3	0.0T
58	0	0	2	2	1	7.1	−7	0.0T	3	0.0T
59	1	0	2	−2	1	23.9	6	0.0T	−3	0.0T
60	0	0	0	−2	1	14.7	−5	0.0T	3	0.0T
61	1	−1	0	0	0	29.8	5	0.0T	0	0.0T
62	2	0	2	0	1	6.9	−5	0.0T	3	0.0T
63	0	1	0	−2	0	15.4	−4	0.0T	0	0.0T
64	1	0	−2	0	0	26.9	4	0.0T	0	0.0T
65	0	0	0	1	0	29.5	−4	0.0T	0	0.0T
66	1	1	0	0	0	25.6	−3	0.0T	0	0.0T
67	1	0	2	0	0	9.1	3	0.0T	0	0.0T
68	1	−1	2	0	2	9.4	−3	0.0T	1	0.0T
69	−1	−1	2	2	2	9.8	−3	0.0T	1	0.0T
70	−2	0	0	0	1	13.7	−2	0.0T	1	0.0T
71	3	0	2	0	2	5.5	−3	0.0T	1	0.0T
72	0	−1	2	2	2	7.2	−3	0.0T	1	0.0T
73	1	1	2	0	2	8.9	2	0.0T	−1	0.0T
74	−1	0	2	−2	1	32.6	−2	0.0T	1	0.0T
75	2	0	0	0	1	13.8	2	0.0T	−1	0.0T
76	1	0	0	0	2	27.8	−2	0.0T	1	0.0T
77	3	0	0	0	0	9.2	2	0.0T	0	0.0T
78	0	0	2	1	2	9.3	2	0.0T	−1	0.0T
79	−1	0	0	0	2	27.3	1	0.0T	−1	0.0T
80	1	0	0	−4	0	10.1	−1	0.0T	0	0.0T
81	−2	0	2	2	2	14.6	1	0.0T	−1	0.0T
82	−1	0	2	4	2	5.8	−2	0.0T	1	0.0T
83	2	0	0	−4	0	15.9	−1	0.0T	0	0.0T
84	1	1	2	−2	2	22.5	1	0.0T	−1	0.0T
85	1	0	2	2	1	5.6	−1	0.0T	1	0.0T
86	−2	0	2	4	2	7.3	−1	0.0T	1	0.0T
87	−1	0	4	0	2	9.1	1	0.0T	0	0.0T
88	1	−1	0	−2	0	29.3	1	0.0T	0	0.0T
89	2	0	2	−2	1	12.8	1	0.0T	−1	0.0T
90	2	0	2	2	2	4.7	−1	0.0T	0	0.0T
91	1	0	0	2	1	9.6	−1	0.0T	0	0.0T
92	0	0	4	−2	2	12.7	1	0.0T	0	0.0T
93	3	0	2	−2	2	8.7	1	0.0T	0	0.0T
94	1	0	2	−2	0	23.8	−1	0.0T	0	0.0T
95	0	1	2	0	1	13.1	1	0.0T	0	0.0T
96	−1	−1	0	2	1	35.0	1	0.0T	0	0.0T
97	0	0	−2	0	1	13.6	−1	0.0T	0	0.0T
98	0	0	2	−1	2	25.4	−1	0.0T	0	0.0T
99	0	1	0	2	0	14.2	−1	0.0T	0	0.0T
100	1	0	−2	−2	0	9.5	−1	0.0T	0	0.0T
101	0	−1	2	0	1	14.2	−1	0.0T	0	0.0T
102	1	1	0	−2	1	34.7	−1	0.0T	0	0.0T
103	1	0	−2	2	0	32.8	−1	0.0T	0	0.0T
104	2	0	0	2	0	7.1	1	0.0T	0	0.0T
105	0	0	2	4	2	4.8	−1	0.0T	0	0.0T
106	0	1	0	1	0	27.3	1	0.0T	0	0.0T

where $\bar{\xi}$ is the vector angle which minimizes

$$\int_{V_E} \rho |\mathbf{s} - \bar{\xi} \times \mathbf{x}|^2 \, dV \tag{3.12}$$

$\bar{\xi}$ is given by the solution to

$$\mathscr{I}_0 \cdot \xi = \int_{V_E} \rho \mathbf{x} \times \mathbf{s} \, dV \tag{3.13}$$

where

$$\mathscr{I}_0 = \begin{pmatrix} A & 0 & 0 \\ 0 & A & 0 \\ 0 & 0 & C \end{pmatrix} \tag{3.14}$$

is the unperturbed inertia tensor of the Earth. This definition of $\bar{\xi}$ is slightly different than a value derived solely from the $\eta(r, \omega)$ component in (3.1). This is because the constant density surfaces in (3.12) and (3.13) are not spherical, but slightly elliptical, and consequently $\bar{\xi}$ is very slightly modified by **b** in (3.1).

The mean rotation vector of any subregion of the Earth may similarly be defined by changing the domain of integration in (3.12) and (3.13) accordingly. We have computed here the mean rotation vector for the mantle ($\mathbf{I}_M$) and for the outer elliptical surface ($\mathbf{I}_s$) as well as for the entire Earth. Differences between these three axes are due predominantly to radial variations in $\eta(r, \omega)$ and particularly to its discontinuity across the core–mantle boundary. The nutational calculations of Molodensky (1961) correspond to $\mathbf{I}_M$.

Figure axis

The Earth's figure axis is defined here as the instantaneous axis of greatest moment of inertia. For an axisymmetric Earth the unperturbed inertia tensor $\mathscr{I}_0$, is given by (3.14). For the forced problem the total inertia tensor is

$$\mathscr{I} = \mathscr{I}_0 + \delta\mathscr{I} \tag{3.15}$$

where $\delta\mathscr{I}$ is related in rectangular coordinates to the complete tidal deformation, **s**, by

$$\delta\mathscr{I}_{ij}(x) = \int_{V_E} \rho \left[2\mathbf{s} \cdot \mathbf{x}\delta_{ij} - (s_i x_j + s_j x_i)\right] \tag{3.16}$$

where δ_{ij} is the Kroenecker delta function.

The instantaneous axis of figure, **F**, must satisfy

$$\mathscr{I} \cdot \mathbf{F} = (C + \delta C)\mathbf{F} \tag{3.17}$$

where $C + \delta C$ is the instantaneous moment of greatest inertia. It is not difficult to show that

$$\mathbf{F} = \hat{\mathbf{z}} + \frac{1}{C - A}\left[\hat{\mathbf{x}}\delta\mathscr{I}_{xz} + \hat{\mathbf{y}}\delta\mathscr{I}_{yz}\right] \tag{3.18}$$

and

$$\delta C = \delta\mathscr{I}_{zz}. \tag{3.19}$$

The diurnal tides do not contribute to δI_{zz}.

F is highly sensitive to the body tide **b** in (3.1). The reason is the small ellipticity of the Earth. On a nearly spherical earth it does not take much deformation to shift the figure axis, since that axis is quite weakly constrained to begin with. This is reflected in (3.18) by the factor $1/(C-A)$. On the other hand, the effect of rigid body rotational motion on **F** is nearly independent of the ellipticity. As a result, the figure axis is usually more a reflection of the elastic behaviour of the Earth than of its rotational motion. The figure axes have, however, been computed for the surface ($\mathbf{F}_s$), the mantle ($\mathbf{F}_M$) and the whole Earth.

Angular momentum

The angular momentum of the Earth is the product of the instantaneous inertia tensor with the instantaneous rotation vector

$$\mathbf{H}_E = \mathscr{I} \cdot \mathbf{I}_E = C\boldsymbol{\Omega} + \delta\mathscr{I} \cdot \boldsymbol{\Omega} + \mathscr{I}_0 \cdot \partial_t \bar{\boldsymbol{\xi}}. \tag{3.20}$$

Similar expressions describe the angular momentum of the mantle, $\mathbf{H}_M$.

Equation (3.20) shows that the angular momentum is affected by changes in the rotation rate (through $\partial_t \bar{\boldsymbol{\xi}}$) and by internal mass redistribution (through $\delta\mathscr{I}$). For $\mathbf{H}_E$ we expect all elastic contributions to cancel leaving a value identical to the rigid body result. (The total angular momentum is a function only of the applied torque.) This offers a means of testing for internal consistency.

Interpretation of **B**

To understand the physical significance of **B**, we introduce the concept of the Tisserand mean (see Munk & MacDonald 1960). Let $\mathbf{I}_M$ be the mean rotation vector of the mantle

$$\mathbf{I}_M = \boldsymbol{\Omega} + \partial_t \bar{\boldsymbol{\xi}}_M \tag{3.21}$$

as described above. The 'Tisserand mean mantle' is defined by conceptually rigidly rotating the mantle from a state of equilibrium with an instantaneous angular velocity of $\mathbf{I}_M$. The axis of figure of the rigidly displaced Tisserand mean mantle is (see equation (2.15))

$$\mathbf{F}_M^{\text{Tiss}} = \hat{\mathbf{z}} + \mathrm{i}\bar{\boldsymbol{\xi}}_M. \tag{3.22}$$

The desired effect of this definition is to rid the Tisserand mantle figure axis of contamination from the body tide deformation. It does not quite realize this objective on an elliptical earth, since the elliptical density distribution used to define $\bar{\boldsymbol{\xi}}_M$ slightly couples the body tide to $\bar{\boldsymbol{\xi}}_M$.

The concept of Tisserand mean can be extended to the outer (elliptical) surface, S, where the axis of figure for the appropriately defined Tisserand mean outer surface is

$$\mathbf{F}_s^{\text{Tiss}} = \hat{\mathbf{z}} + \mathrm{i}\bar{\boldsymbol{\xi}}_s \tag{3.23}$$

with $\bar{\boldsymbol{\xi}}_s$ given by expressions similar to (3.12) and (3.13) ($\int_{V_E}$ replaced by $\int_S$). Once again, $\mathbf{F}_s^{\text{Tiss}}$ is not completely free from body tide effects, since S is slightly elliptical. However, from a practical viewpoint this small elliptical coupling can be ignored and $\bar{\boldsymbol{\xi}}_s$ and $\boldsymbol{\xi}(a, \omega)$, the latter defining the axis **B** in (3.8), can be accepted as equivalent. **B** may then be perceived as essentially the axis of figure for the Tisserand mean outer surface, $\mathbf{F}_s^{\text{Tiss}}$.

Results for the different axes

Nutations for all these axes have been computed for model 1066A for eight important frequencies and are shown in Table 3. Results represent $(a/a_r) - 1$ where a and a_r are the

Table 3. Circular nutation ratios for various axes as computed for earth model 1066A. The results represent $(a/a_r) - 1$, where a and a_r are the circular nutation amplitudes of the given axis for model 1066A and for a rigid earth, respectively. Molodensky's (1961) results are also included. The results for H_E provide an estimate for the numerical error in the other axes.

Nutation frequency	B	I_M	I_E	H_E	H_M	F_M	F_S	I_M Molodensky Model I	I_M Molodensky Model II
1/13.7	0.0283	0.0283	−0.0230	0.00021	0.0488	5.74	4.62	0.026	0.022
1/183	0.0344	0.0344	−0.0015	0.00025	0.0359	0.478	0.394	0.0359	0.0316
1/365	0.0273	0.0273	−0.0007	0.00020	0.0280	0.245	0.205	0.0286	0.0251
1/6800	0.00314	0.00314	−0.00003	0.000023	0.00318	0.0141	0.0123	0.00333	0.00291
−1/6800	−0.00360	−0.00360	0.00002	−0.000026	−0.00364	−0.0144	−0.0126	−0.00383	−0.00334
−1/365	0.246	0.246	0.002	0.0018	0.245	−0.0977	−0.00483	0.247	0.225
−1/183	0.0850	0.0850	0.0023	0.00063	0.0833	−0.418	−0.311	0.0884	0.0786
−1/13.7	0.0724	0.0724	0.0237	0.00055	0.0517	−6.58	−5.27	0.080	0.071

computed results for a non-rigid and rigid earth, respectively. Molodensky's (1961) results for $\mathbf{I}_M$ are included for comparison. Several features deserve discussion.

As discussed above, the $\mathbf{H}_E$ results shown in Table 3 provide an estimate for the absolute errors in the other axes. In most cases this error amounts to approximately 1 or 2 per cent of the total axis ratio. (The absolute errors in the figure axes, $\mathbf{F}_M$ and $\mathbf{F}_S$, are in general somewhat larger due to independent error sources. However, the results in Table 3 for the figure axes should also be accurate to 1 per cent.) Since computation of $\mathbf{H}_E$ involves integration of the tidal solution over the Earth's volume, its magnitude is probably mostly a measure of the accuracy of that integration. Consequently, it provides a fairly conservative error estimate for the non-integration axis, **B**.

Differences between nutations of the various axes generally come from one of two processes: (1) elastic deformation in the mantle, and (2) near resonant excitation of the FCN. The FCN differential rotation between core and mantle is clearly evident in Table 3 by comparing $\mathbf{H}_M$ with $\mathbf{H}_E$ or $\mathbf{I}_M$ with $\mathbf{I}_E$ at any of the tidal lines. The differences are the largest at $-1/365$ which lies very near the FCN eigenfrequency.

The elastic mantle deformation, on the other hand, is particularly evident at those frequencies, such as $\pm 1/13.7$, which are farthest from the FCN eigenfrequency. Here, differences between the mantle angular momentum, $\mathbf{H}_M$, and the mean mantle rotation, $\mathbf{I}_M$, are quite pronounced. In addition, as predicted, the figure axes $\mathbf{F}_M$ and $\mathbf{F}_S$ are strongly perturbed by the mantle deformation at every frequency. They are included in Table 3 strictly for illustrative purposes.

One important but not surprising conclusion can be drawn from the fact that the ratios for **B** and $\mathbf{I}_M$ are identical. This implies that the nutation angle $\eta(r, \omega)$ does not vary significantly throughout the mantle, and that the observable nutations are as well represented by the axis of figure of the Tisserand mean *mantle* as by **B**. However, it should be emphasized that **B** is the more fundamental axis in the sense that if we *had* found a significant difference between the Tisserand mantle and the Tisserand surface, we would have been obliged to adopt the surface axis, **B**, as representative of the Earth's nutation.

3.4 EFFECTS OF DIFFERENT STRUCTURAL MODELS

So far we have only discussed results for structural model 1066A. Table 4 shows results for **B** for the three other models at eight important frequencies. $\mathbf{H}_E$ represents an error estimate, as discussed above. Even assuming that the small differences between results are real (i.e. computationally significant), there is no hope of resolving them observationally. The ratios

Table 4. Circular nutation ratios for the axes **B** and $\mathbf{H}_E$ as computed for three different earth models (corresponding results for model 1066A are included in Table 3). The results shown for **B** represent $[\eta(a, \omega)/\eta_r] - 1$. $\mathbf{H}_E$ corresponds to an absolute error estimate.

Nutation	PEM-C		1066A neutral		1066A stable	
frequency	**B**	$\mathbf{H}_E$	**B**	$\mathbf{H}_E$	**B**	$\mathbf{H}_E$
1/13.7	0.0283	0.00022	0.0284	0.00031	0.0284	0.00032
1/183	0.0344	0.00019	0.0345	0.00027	0.0345	0.00027
1/365	0.0272	0.00015	0.0273	0.00021	0.0273	0.00021
1/6800	0.00314	0.000017	0.00315	0.000024	0.00315	0.000024
−1/6800	−0.00359	−0.000019	−0.00361	−0.000027	−0.00361	−0.000027
−1/365	0.249	0.00133	0.247	0.0019	0.247	0.0019
−1/183	0.0852	0.00045	0.0852	0.00063	0.0852	0.00064
−1/13.7	0.0725	0.00037	0.0725	0.00046	0.0725	0.00045

shown in Table 4 correspond to absolute differences in **B** between structural models of no more than 0.0001 arcsec at individual frequencies. This is well below any projected measurement accuracy in the foreseeable future.

3.5 COMPARISON WITH OTHER RESULTS

Table 5 compares the basic theoretical assumptions of our theory with those of Molodensky (1961) and Shen & Mansinha (1976). The development of Sasao *et al.* (1980) is similar to Molodensky's except that Sasao *et al.* use the complete non-static Louisville equation to describe conservation of angular momentum. The spheroidal and toroidal fields referred to in Table 5 are simply collections of displacement scalar functions and are described for this problem by Wahr (1981b); τ_1^1 represents a nutational displacement of the form $\eta(r)\,(\hat{\mathbf{x}} + i\hat{\mathbf{y}}) \times \mathbf{x}$ and σ_2^1 and τ_3^1 represent tidal deformation. The complete solution for an elliptical, rotating earth contains an infinite number of τ^s and σ^s.

An apparently more important source of disagreement between results is due to the structural models used. Our results indicate that there is probably little difference between results for different contemporary models. However, since earth models improved rapidly in the early 1970s, there is no reason to assume that theories which use older structural models do not contain model related deficiencies. This may be particularly true for Molodensky's (1961) results.

The effects of the recent improvement in structural models are clearly evident when results of non-rigid nutation theories are compared, as in Figs 5 and 6, for $(\eta/\eta_\tau) - 1$ and $\delta\epsilon$, $\delta\psi$, respectively. Agreement between theories based on modern earth models is uniformly very good (with the exception of an anomalously large Shen & Mansinha (1976) value at $-1/13.7$ in Fig. 5). Molodensky's model II, however, systematically diverges from the more modern theories by up to 0.002 arcsec at six month and at 18.6 yr. Especially striking is the close agreement between the modern theories and Molodensky's theory as recomputed by Shen & Mansinha (1976) for the earth model of Pekeris & Accad (1972). It thus seems inescapable that Molodensky's results suffer the effects of a structural model which is nearly two decades old.

Table 5. A comparison of the physical limitations and analytical assumptions of different nutation theories for a non-rigid earth. τ and σ represent toroidal and spheroidal displacements.

	Molodensky (1961)	Shen & Mansinha (1976)	Wahr (present theory)
Mantle and inner core	Rotation and deformation are separated. Deformation is computed using static equations for a spherical, non-rotating elastic body. The solution is truncated to: σ_2^1	Rotation and deformation are separated. Deformation is computed using equations for a spherical, non-rotating elastic body. The solution is truncated to: σ_2^1	Rotation and deformation are computed simultaneously. Elliptical and rotational effects are considered throughout the (elastic) material and at all boundaries. The solution is truncated to: $\tau_1^1 + \sigma_2^1 + \tau_3^1$
Fluid core	Rotation and deformation are separated. Deformation is computed using static equations for a spherical, non-rotating fluid core. The solution is truncated to: $\tau_1^1 + \sigma_2^1$	Rotation and deformation are computed simultaneously. Elliptical and rotational effects are considered throughout the fluid core. However, elliptical effects are not included at the boundaries. The solution is truncated to: $\tau_1^1 + \sigma_2^1 + \tau_3^1$	Rotation and deformation are computed simultaneously. Elliptical and rotational effects are considered throughout the fluid core and at all boundaries. The solution is truncated to: $\tau_1^1 + \sigma_2^1 + \tau_3^1$

	1/13.7	1/183	1/6800	- 1/6800	- 1/183	- 1/13.7
M	.022	.0316	.00291	-.00334	.0786	.071
SOS	.028	.035	.0032	-.0037	.085	.073
MSM	.0282	.0345	.00317	-.00364	.0841	.0722
SM	.0286	.0359	.00329	-.00378	.0883	.0762
W	.0283	.0344	.00314	-.00360	.0850	.0724

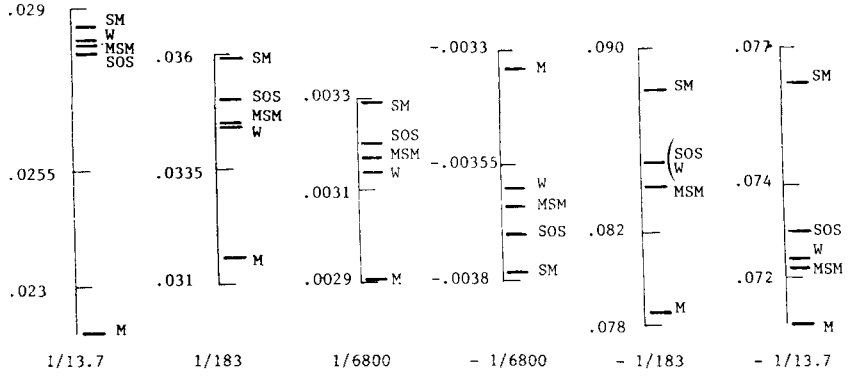

M : Molodensky (1961) model II
SM : Shen and Mansinha (1976) using model of Pekeris and Acad (1972) . β=0 .
MSM : Molodensky's theory recomputed by Shen and Mansinha (1976) for the Earth model of Pekeris and Acad (1972) .
SOS : Sasao, et al (1980) using Wang's (1972) model.
W : Wahr's results (this paper) using model 1066A from Gilbert and Dziewonski (1975).

Figure 5. Circular nutation amplitude ratios (see text) are compared for different non-rigid theories.

	Rigid Earth values Kinoshita 2000	M	SOS	MSM	SM	W
18.6 year Δε	9.2278	9.2044	9.2018	9.2022	9.2012	9.2025
ΔΨ sin ε	-6.8743	-6.8441	-6.8407	-6.8413	-6.8400	-6.8416
semiannual Δε	0.5534	0.5719	0.5739	0.5736	0.5745	0.5736
ΔΨ sin ε	-0.5082	-0.5232	-0.5249	-0.5246	-0.5253	-0.5245
fortnightly Δε	0.0949	0.0972	0.0977	0.0977	0.0978	0.0977
ΔΨ sin ε	-0.0881	-0.0899	-0.0904	-0.0904	-0.0904	-0.0905

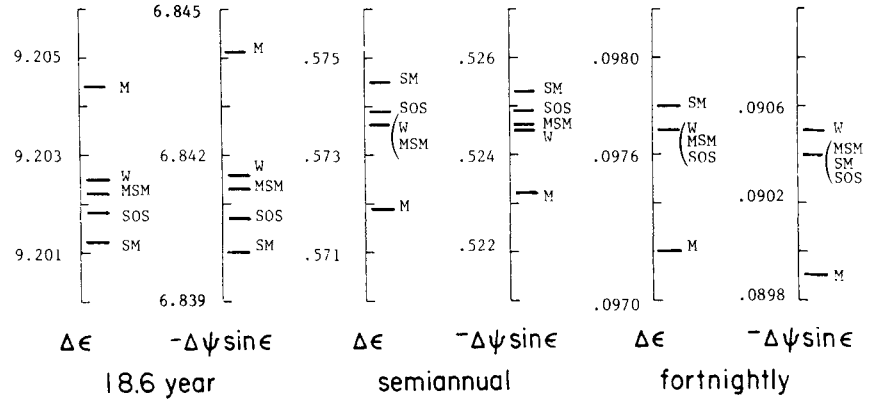

Figure 6. Nutational variations in ecliptic longitude and obliquity are shown in arcseconds for different theories. All non-rigid results are computed by convolving with the results from Kinoshita's rigid earth theory for the epoch 2000 (see Kinoshita *et al.* 1979). The different theories are identified in Fig. 5.

4 Discussion

Our principal motivation was to determine whether observations of the Earth's nutation can extend our knowledge of the Earth's material structure, most notably of the poorly determined stability of the fluid core. The total correction to the nutation for a realistic model of the Earth's non-rigidity is quite large (i.e. a displacement of the pole by 0.02 arcsec at six month and at 18.6 yr) and is consistent with the observed results (Fig. 4).

Differences between our results and the earlier, well-known results of Molodensky (1961) are about 10 per cent of the total non-rigid correction, or 0.002 arcsec at six month and 18.6 yr. These differences are due to deficiencies in Molodensky's two-decade-old structural model of the Earth and, to a lesser extent, to extensions in the present theory. A perturbation of 0.002 arcsec is slightly larger than the dynamical effect of the oceans on the nutations (Wahr & Sasao 1981) and probably larger than the effects of dissipative core–mantle coupling (Toomre 1974; Sasao *et al.* 1977). At present, conventional astronomic observations disagree by more than 0.002 arcsec (Fig. 4), although statistical errors claimed for individual measurements are often below 0.002 arcsec. Furthermore, new astrometric techniques, such as VLBI (Counselman 1976; Carter 1978) and laser ranging (Smith *et al.* 1978; Silverberg 1978), promise to achieve an accuracy of better than 0.002 arcsec in the next few years.

For the different contemporary structural models considered here, the nutation results are in good agreement. Differences at specific frequencies are no larger than 0.0001 arcsec which is well below any foreseeable future accuracy. This implies that observations of the forced nutations will be unable to differentiate between these elastic structural models. In particular, there is little hope of extending our knowledge of the core stability. On the other hand, this close agreement suggests that our results adequately represent the nutation of an elastic, hydrostatically prestressed and oceanless earth. Consequently, they can be used with considerable confidence to 'correct' astrometric data for the nutation of such an earth, in order to study other effects.

Acknowledgments

I am greatly indebted to M. L. Smith; without his help and encouragement this work would not have been possible. I thank T Sasao and P. Bender for many long discussions and invaluable suggestions. It was T. Sasao who first noticed the effects of structural models on the older nutation theories. T. Sasao also initially organized Figs 5 and 6 and Table 5 of this paper. I thank B. Sloan for her preparation of the manuscript. Financial support was provided by CIRES and by the National Aeronautics and Space Administration under grant NSG 7319.

References

Atkinson, R. d'E., 1973. On the 'dynamical variation' of latitude and time, *Astr. J., N.Y.*, **78**, 147–151.

Atkinson, R. d'E., 1975. On the Earth's axes of rotation and figure, *Mon. Not. R. astr. Soc.*, **71**, 381–386.

Bartels, J., 1957. Geszeitenkrafte, in *Encyclopedia of Physics*, Vol. 48 (Geophysics II), pp. 734–774, Springer-Verlag, Berlin.

Brown, E. W., 1919. *Tables of the Motion of the Moon*, Yale University Press, New Haven.

Carter, W. E., 1978. Modern methods for the determination of polar motion and UT1, presented at *IAU Symp. No. 82*, Time and the Earth's Rotation, Cadiz, Spain, May 1978.

Cartwright, D. E. & Tayler, R. J., 1971. New computations of the tide-generating potential, *Geophys. J. R. astr. Soc.*, **23**, 45–74.

Counselman II, C. C., 1976. Radio astrometry, *Ann. Rev. Astr. Astrophys.*, **14**, 197–214.

Dahlen, F. A. & Smith, M. L., 1975. The influence of rotation on the free oscillations of the Earth, *Phil. Trans. R. Soc.*, **279A**, 583–624.

Dziewonski, A. M., Hales, A. L. & Lapwood, E. R., 1975. Parametrically simple Earth models consistent with geophysical data, *Phys. Earth planet. Int.*, **10**, 12–48.

Gilbert, F. & Dziewonski, A. M., 1975. An application of normal mode theory to the retrieval of structural parameters and source mechanisms from seismic spectra, *Phil. Trans. R. Soc.*, **278A**, 187–269.

Jeffreys, H., 1959. Nutation: comparison of theory and observations, *Mon. Not. R. astr. Soc.*, **119**, 75–80.

Jeffreys, H., 1970. *The Earth*, 5th edn, Cambridge University Press.

Jeffreys, H. & Vicente, R. O., 1957a. The theory of nutation and the variation of latitude, *Mon. Not. R. astr. Soc.*, **117**, 142–161.

Jeffreys, H. & Vicente, R. O., 1957b. The theory of nutation and the variation of latitude: the Roche model core, *Mon. Not. R. astr. Soc.*, **117**, 162–173.

Kinoshita, H., 1977. Theory of the rotation of the rigid Earth, *Cel. Mech.*, **15**, 277–326.

Kinoshita, H., Nakajima, K., Kubo, Y., Nakagawa, I., Sasao, T. & Yokoyama, K., 1979. Note on nutation in ephemerides, *Publs int. Latit. Obs. Mizusawa*, **12**, 71–108.

Masters, G., 1979. Observational constraints on the chemical and thermal structure of the earth's deep interior, *Geophys. J. R. astr. Soc.*, **57**, 507–534.

Melchior, P., 1971. Precession-nutations and tidal potential, *Cel. Mech.*, **4**, 190.

Melchior, P., 1978. *The Tides of the Planet Earth*, Pergamon Press, Oxford.

Molodensky, M. S., 1961. The theory of nutation and diurnal Earth tides, *Communs Obs. R. Belg.*, **288**, 25–56.

Munk, W. H. & MacDonald, G. J. F., 1960. *The Rotation of the Earth*, Cambridge University Press, London.

Pekeris, C. L. & Accad, Y., 1972. Dynamics of the liquid core of the Earth, *Phil. Trans. R. Soc.*, **273A**, 237–260.

Poincare, H., 1910. Sur la precession des corps deformables, *Bull. Astr.*, **27**, 321–356.

Sasao, T., Okamoto, J. & Sakai, S., 1977. Dissipative core–mantle coupling and nutational motion of the Earth, *Publs astr. Soc. Japan*, **29**, 83–105.

Sasao, T., Okubo, S. & Saito, M., 1980. A simple theory on dynamical effects of stratified fluid core upon nutational motion of the earth, *Proc. IAU Symp. No. 78*, Nutation and the Earth's Rotation, Kiev, May 1977, eds Fedorov, E. P., Smith, M. L. & Bender, P. L.

Shen, P.-Y. & Mansinha, L., 1976. Oscillation, nutation, and wobble of an elliptical rotating Earth with liquid outer core, *Geophys. J. R. astr. Soc.*, **46**, 467–496.

Silverberg, E. C., 1978. On the effective use of lunar ranging for determination of the Earth's orientation, presented at *IAU Symp. No. 82*, Time and the Earth's Rotation, Cadiz, Spain, May 1978.

Smith, D. E., Kolenkiewicz, R., Dunn, P. J. & Torrence, M., 1978. Determination of polar motion and Earth rotation from laser tracking of satellites, presented at *IAU Symp. No. 82*, Time and the Earth's Rotation, Cadiz, Spain, May 1978.

Smith, M. L., 1974. The scalar equations of infinitesimal elastic-gravitational motion for a rotating, slightly elliptical earth, *Geophys. J. R. astr. Soc.*, **37**, 491–526.

Smith, M. L., 1976. Translational inner core oscillations of a rotating, slightly elliptical earth, *J. geophys. Res.*, **81**, 3055–3065.

Smith, M. L., 1977. Wobble and nutation of the Earth, *Geophys. J. R. astr. Soc.*, **50**, 103–140.

Smith, M. L. & Dahlen, F. A., 1981. The period and Q of the Chandler wobble, *Geophys. J. R. astr. Soc.*, **64**, 223–281.

Toomre, A., 1974. On the 'nearly diurnal wobble' of the Earth, *Geophys. J. R. astr. Soc.*, **38**, 335–348.

Wahr, J. M., 1981a. A normal mode expansion for the forced response of a rotating earth, *Geophys. J. R. astr. Soc.*, **64**, 651–675.

Wahr, J. M., 1981b. Body tides on an elliptical, rotating, elastic and oceanless earth, *Geophys. J. R. astr. Soc.*, **64**, 677–703.

Wahr, J. M. & Sasao, T., 1981. A diurnal resonance in the ocean tide and in the Earth's load response due to the resonant free 'core nutation', *Geophys. J. R. astr. Soc.*, **64**, 747–765.

Wahr, J. M., 1981b. Body tides on an elliptical, rotating, elastic and oceanless earth, *Geophys. J. R.* to long period tides, *Geophys. J. R. astr. Soc.*, **64**, 635–650.

Wang, C. Y., 1972. A simple Earth model, *J. geophys. Res.*, 77, 4318.

Woolard, E. W., 1953. Theory of the rotation of the earth around its center of mass, *Astr. Pap. Wash.*, **15**, Vol. XV, part 1.